Fracture behaviour, microstructure, and performance of various layered-structured Al_2O_3-TiC-WC-Co composites

Changxia Liu [a,b*] Junlong Sun [a, b*] Chao Wang [a*] Fengxun Li [a] Tanvir Hussain [b]

[a] School of Transportation, Ludong University, Yantai 264025, Shandong Province, P.R. China

[b]Faculty of Engineering, University of Nottingham, University Park, Nottingham, NG7 2RD，UK.

Abstract: In this study, layered-structured Al_2O_3-based composites containing WC-Co, TiC, and MgO additives were prepared using hot-pressing sintering. The best comprehensive mechanical characteristics were acquired for the sample with a layer number (N_{LN}) of 7 and thickness ratio (η_{TR}) of 6. Its composite exhibited a fracture toughness of 8.5 and 8.4 MPa·$m^{1/2}$ in the *X* and *Z* directions, respectively. Analysis of the micro characteristics of the fracture surfaces of the Al_2O_3-TiC-WC-Co layered composites revealed a significant enhancement in the bending strength, which could be attributed to the mixed fracture modes in the composite, including intergranular and trans-granular modes. As the displacement increased, first, the bending stress of all the composites increased gradually, after which all the samples showed abrupt elevation in stress. The enhancement in the damage resistance of Al_2O_3-TiC-WC-Co layered composites could be attributed to the microscopic and macroscopic crack deflection, bridging, and partial surface bonding that occurred in the layers. Finally, a new theoretical perspective was employed to discuss the mechanism of the effect of the layered structure on the toughness of the composites.

Keywords: Fracture behaviour; Microstructure; Mechanical property; Alumina; Layered

1. Introduction

Alumina has attracted significant attention for various applications in the engineering field owing to its high hardness, low specific weight, thermal stability, and excellent corrosion and wear resistance. However, its inherent disadvantages, such as high brittleness and low bending strength, have limited its applications. Among the approaches for enhancement of fracture behaviour, the layered structure has emerged as an effective method for addressing the limitations of alumina [1]. For example, a layered structure effectively suppresses the catastrophic fractures of alumina by enhancing its defect tolerance, which is important in extreme applications, such as in hypersonic aircraft long-haul flights and atmospheric re-entry of space vehicles [2, 3].

Several studies have investigated layered composites [2, 4, 5]. For example, a previous study demonstrated that the bending strength of ZrB_2-SiC_w/BN layered composite at room temperature was as high as 425±19 MPa[2] (SiC_w means SiC whisker). Layered-structured composites prepared by hot-pressing sintering and

*Corresponding author.
liuchangxia2013@126.com (ChangxiaLiu); sjlthink@163.com (Junlong Sun); 350386167@qq.com(Chao Wang)

other processes exhibit attractive inherent advantages. For example, the strength and toughness of layered-structured B_4C/TiC composites prepared by a reactive melt infiltration technique can be as high as 160 ± 2 MPa and 5 ± 0.3 MPa·$m^{1/2}$, respectively [1]. In addition, TiB_2-based layered composites fabricated by the centrifugal casting process can achieve a laminar shear strength of 425±50 MPa[6]. Furthermore, layered-structured composites exhibit excellent performance in high-temperature environments. For example, a previous study reported that the strength of ZrB_2-SiC-BN layered composite at 1500 °C was 111 MPa and that of layered-structured ZrB_2-SiC-graphite composites was as high as 377 MPa at the same temperature [7]. Compared to the common layered-structured composites, micro-thick layered-structured composites exhibit better performance. For example, owing to its micro-thickness, the toughness of the micro-thick layered-structured metal ceramic composites (24.78 ± 0.71 MPa·$m^{1/2}$) is significantly higher than those of ordinary ceramic composites [8]. In addition, the fracture toughness of micro-thick (SiC_w+SiC_p)/SiC layered composites is as high as 7.49 MPa·$m^{1/2}$ [9] (SiC_P means SiC particle). Generally, layered-structured composites are prepared via tape casting; however, this method requires high preparation costs and leads to anisotropy of the prepared composites, thus limiting its further application. For example, the bending strength of ZrB_2-SiC/graphite layered composite exhibits anisotropy in the parallel and perpendicular directions (360 and 399 MPa, respectively) [10]. Nevertheless, the layered structure of TiB_2 layered composites improves their thermal shock resistance [11].

The difference in coefficient of thermal expansion (CTE) of the Al_2O_3, TiC, and WC additives in Al_2O_3-TiC-WC composites induces residual stress in the composite, which results in high wear resistance and improved mechanical properties [6, 8, 12]. The addition of Co to Al_2O_3-TiC-WC composites can blunt the crack tip and improve the toughness of the composite owing to its high ductility [8, 13]. In this study, the structural layered design, microstructure, and performance, particularly, the fracture behaviour of the Al_2O_3-TiC-WC-Co layered composites in different directions, were analysed and characterised. Lastly, a new theoretical perspective was utilised to explore the effect of the layered structure of the Al_2O_3-TiC-WC-Co composite on its fracture behaviour.

2. Materials and experimental process

2.1. Design and preparation of the Al_2O_3-TiC-WC-Co layered composite

In this study, α-Al_2O_3 powder (99.9% purity, circular shape and particle diameter of 0.5 μm) (Zibo Lucky Star Ceramics Co., Ltd., China) was used as the matrix material. WC-Co (99% purity, circular shape and

particle diameter of 60 nm), TiC (96% purity, circular shape and particle diameter of 1–3 μm), and MgO powder (98.5% purity, circular shape and particle diameter of 0.5 μm) were used as the additives (manufactured by Nanjing Hongwu Nano Co., Ltd., China). MgO powder was expected to inhibit abnormal grain growth of alumina. Two composite powders (A_W and A_T) were prepared by mixing different proportions of the additives and matrix, and the contents of the two powders are listed in Table 1.

Table1 Contents of the prepared Al_2O_3-TiC-WC-Co layered composite powders

No.	Content wt.%			
	Al_2O_3	WC-Co	TiC	MgO
A_W	94	5	0	1
A_T	79	0	20	1

Briefly, the admixed powders were milled for 120 h in alcohol using planetary ball milling with alumina balls. The dimension of the alumina milling container was Ø100×150 mm^2, and the rotary velocity of the ball milling was adjusted to 50 rpm. The diameter of the alumina ball was 6 mm, the weight ratio of the balls to admixed powders was 1 to 3. The layered structure of the prepared Al_2O_3-TiC-WC-Co composite samples is shown in Fig. 1. The milled powders (*i.e.*, A_W and A_T, with a circular shape and particle diameter of 0.3–1 μm) were placed in a graphite mould according to the sequence and thickness shown in Fig. 1 and Table 2, respectively. Seven samples (SA1–SA7) with different A_T/A_W thickness ratios (η_{TR}) and layer numbers (N_{LN}) were prepared. Subsequently, the graphite mould containing the powders was placed in a hot-pressing furnace and sintered at 1650 °C. The pressure in the furnace increased with increasing sintering temperature. When the desired temperature (1650 °C) was reached, the pressure of 35 MPa in the furnace was maintained for 60 min. An extensive description of the preparation process can be found in a previous study [14].

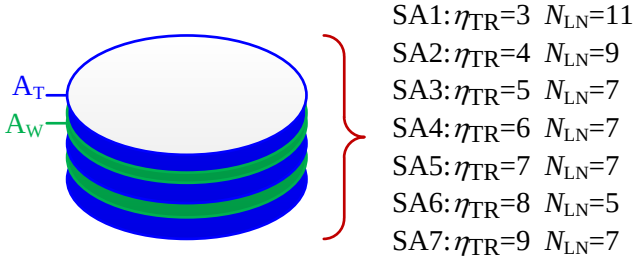

Fig. 1 Structural layered design of Al_2O_3-TiC-WC-Co composites with different A_T/A_W thickness ratios

(η_{TR}) and layer numbers (N_{LN}) (SA1–SA7: prepared samples)

Table 2 The thickness of A_T and A_w layers

No.	A_W	A_T
SA1	0.25 mm	0.75 mm
SA2	0.25 mm	1 mm
SA3	0.25 mm	1.25 mm
SA4	0.25 mm	1.5 mm
SA5	0.2 mm	1.4 mm
SA6	0.2 mm	1.6 mm
SA7	0.2 mm	1.8 mm

2.2. Property testing and microstructural observation

For the property testing and microstructural observation, the as-sintered samples of Al_2O_3-TiC-WC-Co composite were cut into long strips using an internal circular slicer. The bending strength of the samples was measured using a three-point bending test from two directions, indicated as *X* and *Z* directions in Fig. 2, to determine the anisotropy of the composites. The three-point bending test was conducted over a span (*L*) of 25 mm at a moving speed of 0.5 mm/min. The diameter of the mandrel and supports was 5 mm. The force (*P*) at which the specimen fractured was recorded and substituted into the following formula to calculate the bending strength (σ_f) of the corresponding specimen [15].

$$\sigma_f = \frac{3PL}{2bh^2}, \quad (1)$$

b and *h* are marked in Fig. 2.

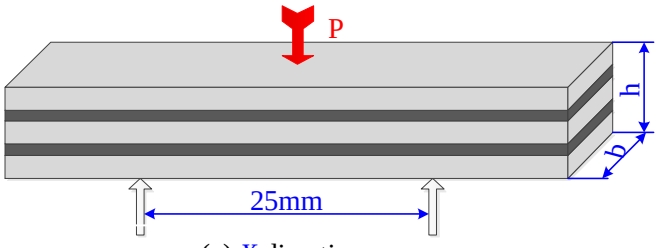

(a) *X* direction

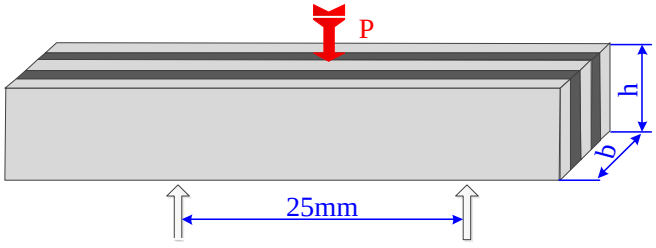

(b) *Z* direction

Fig. 2 Directions (*X* and *Z*) used during the three-point bending test (3 mm × 4 mm × 36 mm)

The micro-Vickers hardness and fracture toughness (K_{IC}) of the samples were measured using the indentation method (HV1 for hardness and HV10 for toughness). The Vickers hardness of the samples was tested at a loading force of 9.8 N, and the force was maintained for 5 s before releasing. The K_{IC} of the samples was determined at a loading force (P_{IC}) of 98 N, and the force was held for 30 s before releasing to generate a crack on the polished surface. K_{IC} was calculated using the following formula [16]:

$$K_{IC} = 0.203a^{\frac{1}{2}}\left(\frac{c}{a}\right)^{-\frac{3}{2}} \cdot 1.8544\frac{P_{IC}}{(2a)^2}, \quad (2)$$

where a and c are the half-length in the diagonal direction and total crack growth length, respectively, as is shown in Fig 3(a). To obtain the Vickers hardness and fracture toughness of both A_T and A_W layers, the indentations were made on the polished top surface of the Z directions, as is shown in Fig. 3(b). A minimum of 12 indentations was used for the Vickers hardness and toughness testing of the Al_2O_3-TiC-WC-Co layered composites to reduce data scattering.

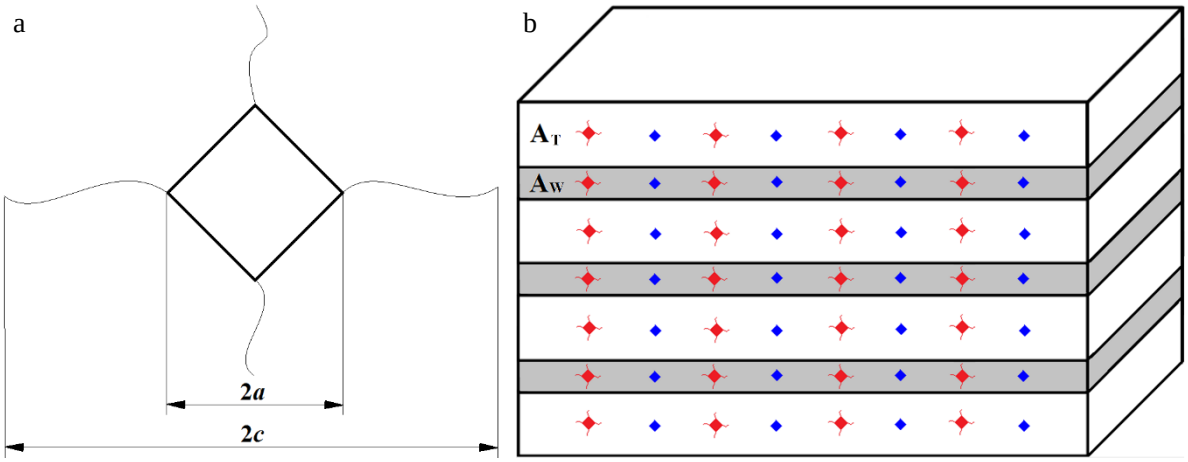

Fig. 3 Schematic diagram of the indentation and cracks (a) and the testing positions of the hardness and toughness in the A_W and A_T layers (b)

The fracture behaviour of the Al_2O_3-TiC-WC-Co layered composites was analysed using the indentation bending strength technique. During the testing, a load of 9.8–98 N was applied and maintained for 15 s before releasing. The samples were tested at least three times, and the average value was calculated. The fracture behaviour of the Al_2O_3-TiC-WC-Co layered composites was explained according to the theory proposed by Braun et al. [15], which states that a radial crack is generated in a sample subjected to a load of P_{Fb}. The stress intensity (K_{SIN}) at the crack tip was calculated using the following formula [17–20]:

$$K_{SIN} = K_{SIA} + K_{RTF} + K_{MSH} = \psi \times \sigma_A \times c_{PFB}^{1/2} + \chi \times P_{Fb}/c_{PFB}^{3/2} + K_{MSH}, \quad (3)$$

where K_{SIA}, K_{RTF}, and K_{MSH} are the stress intensities related to the applied stress (σ_A), the residual touching field at a load of P_{Fb}, and microstructural shielding, respectively. ψ is a coefficient determined using a penny-shape crack, $\chi = \xi (E/H)^{1/2}$ is a coefficient representing the intensity of the residual field, which is ideally independent of the crack size (c_{PFB}), E is Young's modulus, and ξ is a constant. The K_{MSH} value was too small to be neglected [21].

The residual stresses, σ_{RAW} and σ_{RAT}, in the A_W and A_T layers, respectively, were estimated using the following formula [22–24]:

$$\sigma_{RAT} = \frac{\int_{T_{SF}}^{T_0} (\alpha_{AW} - \alpha_{AT}) dT}{\frac{1}{E_{AT}} + \frac{1}{E_{AW}} \times L_v}, \quad (4)$$

$$\sigma_{RAW} = -\sigma_{RAT} \times L_v, \quad (5)$$

where E_{AW} and E_{AT} are Young's moduli and α_{AW} and α_{AT} are the CTEs of the A_W and A_T layers, respectively. In addition, T_0= 15 °C and T_{SF} is the temperature (1200 °C) at which the stress was completely released. L_v is the ratio of the volume of the A_T layer to that of the entire layered structure, and was estimated using η_{TR} and N_{LN} based on the following formula:

$$L_v = \eta_{TR} \times (N_{LN}+1)/(N_{LN}-1), \quad (6)$$

The microstructure of the fracture surfaces and the cracks on the polished surfaces of the Al_2O_3-TiC-WC-Co layered composites were identified using scanning electron microscopy (SEM; HITACHI SU8010, Japan). The macroscopic fracture of the Al_2O_3-TiC-WC-Co layered composite was observed using an optical microscope.

3. Results and discussion

3.1. Analysis of the mechanical performance

The bending strength, fracture toughness, and hardness of the as-sintered Al_2O_3-TiC-WC-Co layered composite samples are listed in Table 3. The bending strengths of samples in both *X* and *Z* directions increased with an increase in η_{TR} from 3 to 6 and decreased with a further increase in η_{TR} from 7 to 9. In addition, SA4 (N_{LN} = 7, η_{TR}= 6) exhibited bending strengths of 460 and 450 MPa in the *X* and *Z* directions, respectively, which were higher than those of the other samples. The effect of layered structure on the toughness of the Al_2O_3-TiC-WC-Co composite was similar to that on the strength. The toughness values of the A_T and A_W layers of SA4 were 8.5 and 8.4 MPa·$m^{1/2}$, respectively, which were higher than those of the other samples. In addition, compared to the findings of previous studies [21, 25], the toughness of the

Al_2O_3-TiC-WC-Co layered composites was higher than that of the un-laminated Al_2O_3-TiC composite. In contrast, SA5 (N_{LN} = 7, η_{TR} = 7) exhibited a Vickers hardness of 24.3 and 23.9 GPa in the A_T and A_W layers, respectively, which were higher than those of the other samples. These results imply that SA4 exhibited better comprehensive mechanical properties than the other samples. This indicates that the optimal η_{TR} and N_{LN} of the Al_2O_3-TiC-WC-Co layered composites were 6 and 7, respectively.

The relatively lower hardness of SA4 in the A_T and A_W layers could be attributed to the fact that the bending strength and fracture toughness of the ceramic composite were closely related to the fracture mode, whereas the hardness was mainly related to the grain size and porosity. This implies that the layered structure effectively improves the fracture mode of the composite [2–10]; however, it does not have a significant effect on the grain size and porosity.

Table 3 Mechanical performance of the Al_2O_3-TiC-WC-Co layered composite samples

No.	Bending strength (MPa)		Fracture toughness (MPa·m$^{1/2}$)		Vickers hardness (GPa)	
	X	*Z*	A_T	A_W	A_T	A_W
SA1	320 ± 21	300 ± 22	6.1 ± 0.8	4.9 ± 0.4	21.8 ± 0.9	21.4 ± 0.3
SA2	400 ± 26	375 ± 23	7.3 ± 0.7	7.3 ± 0.2	20.4 ± 0.2	21.6 ± 0.9
SA3	430 ± 31	420 ± 25	7.4 ± 0.4	6.7 ± 0.6	22.3 ± 0.9	22.0 ± 0.4
SA4	460 ± 25	450 ± 24	8.5 ± 0.3	8.4 ± 0.4	21.5 ± 0.3	22.2 ± 0.2
SA5	440 ± 22	420 ± 27	7.2 ± 0.7	7.5 ± 0.4	24.3 ± 0.6	23.9 ± 0.5
SA6	350 ± 23	330 ± 33	7.6 ± 0.2	6.0 ± 0.3	21.7 ± 0.5	20.5 ± 0.6
SA7	360 ± 20	320 ± 36	6.9 ± 0.3	6.9 ± 0.3	20.0 ± 0.4	21.3 ± 0.6

3.2. Analysis of the residual stresses

The E_{AW} and α_{AW} and E_{AT} and α_{AT} of the A_W and A_T layers, respectively, which were calculated using the mixing rule [14], are listed in Table 4. The residual stresses calculated using formulas (4) and (5) are listed in Table 5. The residual stress in the A_W layers was approximately 400 MPa. In addition, the residual tensile stress in the A_T layers ranged from 34 to 96 MPa (Table 5). The residual tensile stress in the A_T layer resulted in a straight crack propagation path, which was short and consumed small energy. In contrast, the residual compressive stress in the A_W layer resulted in a notable deflection of the expansion path, thus leading to the consumption of more energy. These results indicate that the enhancement in the strength and

toughness of the Al_2O_3-TiC-WC-Co layered composites could be attributed to the presence of the compressive residual stress (Table 5), which is consistent with the findings of previous studies [3–6, 26].

Table 4 Young modulus (E_{AW} and E_{AT}) and coefficient of thermal expansion (α_{AW} and α_{AT}) of the A_W and A_T layers

	A_W	A_T
E_{AW}/E_{AT} (GPa)	380	363
α_{AW}/α_{AT} (10^{-6} K^{-1})	6	7

Table 5 Residual stresses in the A_T and A_W layers of the samples

	SA1	SA2	SA3	SA4	SA5	SA6	SA7
A_T/A_W thickness ratio (η_{TR})	3	4	5	6	7	8	9
A_T Residual tensile stress (MPa)	96	74	58	50	43	34	34
A_W Residual compressive stress (MPa)	–346	–372	–389	–398	–405	–414	–414

3.3 Microstructures

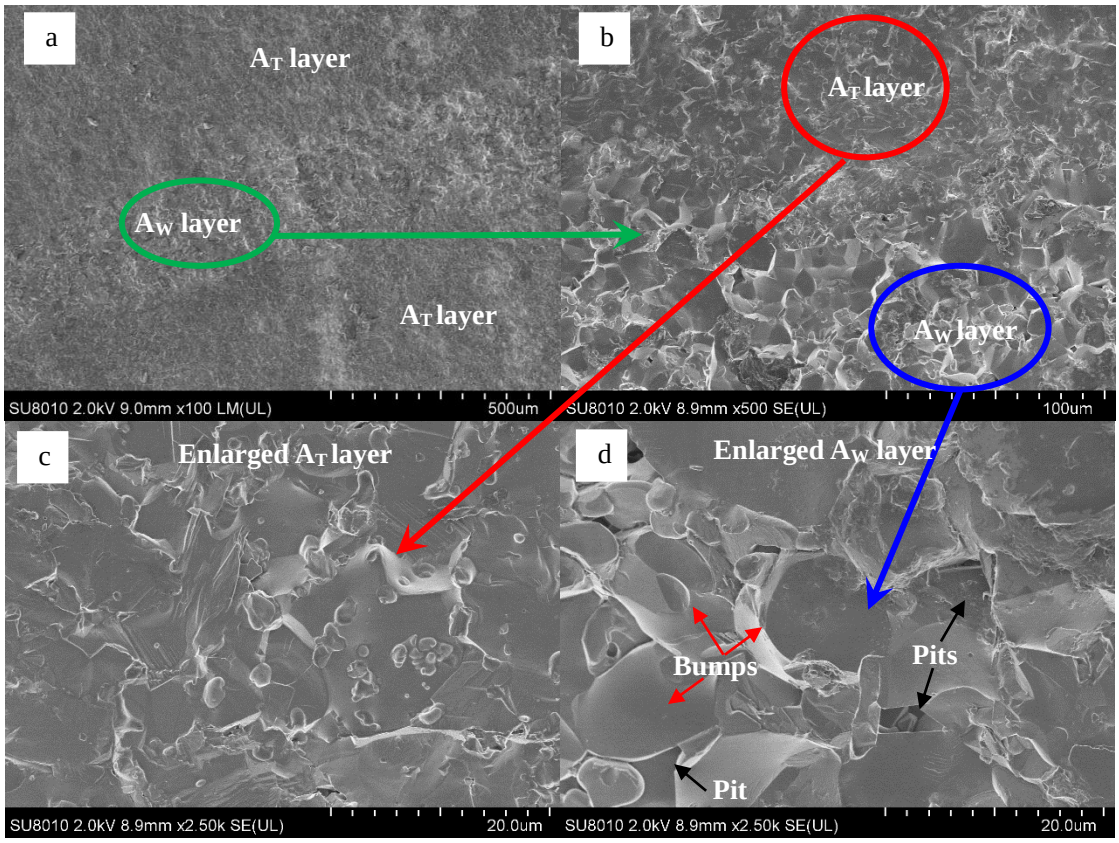

Fig. 4 SEM showing the fracture morphology of SA4 (N_{LN} = 7, η_{TR} = 6): (a) low-magnification SEM image; (b) high-magnification SEM image; (c) enlarged A_T layer, and (d) enlarged A_W layer

Fig. 4 shows the fracture morphology of SA4. A transparent interface was present between the A_W and A_T layers, which possessed different microstructures. A high-resolution image of the green circled area in Fig. 4(a) is shown in Fig. 4(b). Figs. 4(c) and (d) show high-resolution SEM images of the A_T and A_W layers, respectively. Several bumps and pits were observed on the surface of the A_W layer (Fig. 4(c)). In contrast, there were almost no bumps and pits on the surface of the A_T layer, resulting in indistinguishable grain boundaries (Fig. 4(d)).

In addition, the intergranular collapse was the main rupture pattern of the A_W layer (Fig. 4(d)), whereas trans-granular collapse was the main rupture pattern of the A_T layer (Fig. 4(c)). Furthermore, the A_W layer exhibited a regular grain profile with clear grain boundaries (Fig. 4(d)), whereas the A_T layer exhibited irregular grain profiles and indistinguishable grain boundaries (Fig. 4(c)). Consequently, the combination of the intergranular (A_W layer) and trans-granular (A_T layer) collapse rupture pattern improved the strength of the Al_2O_3-TiC-WC-Co layered composites.

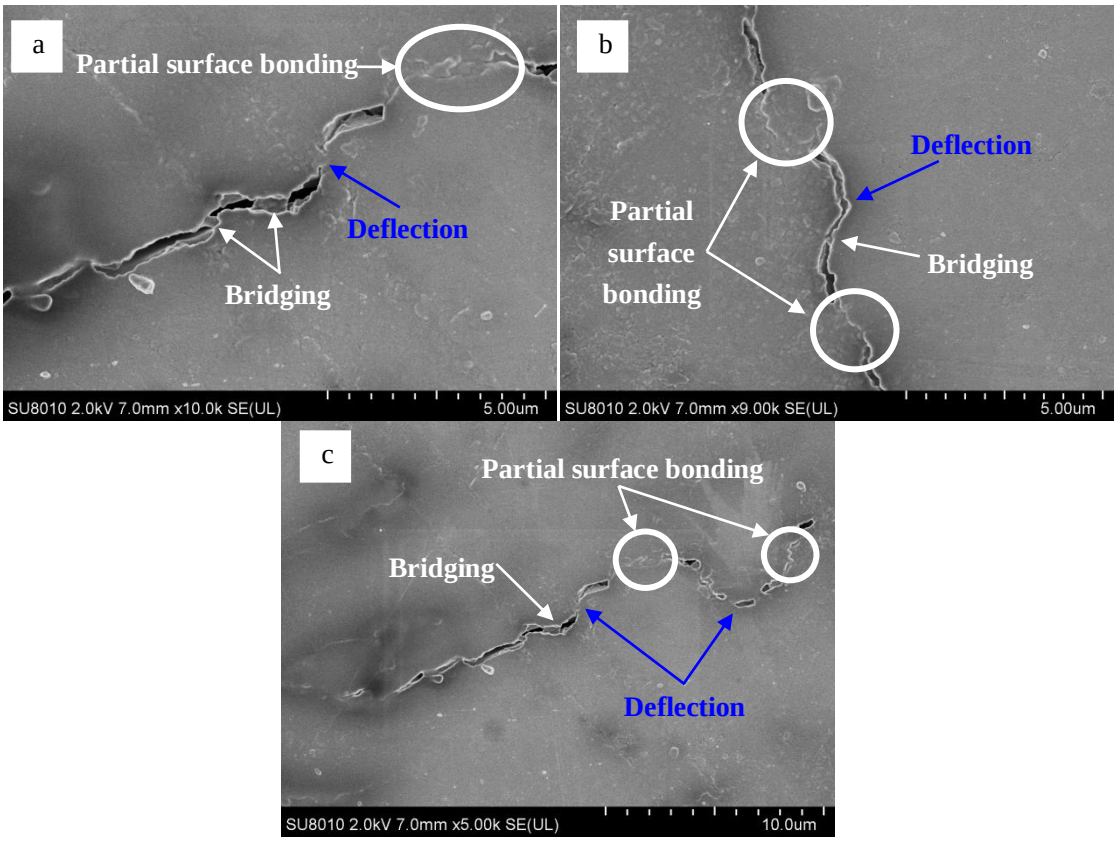

Fig. 5 SEM images showing the cracks on the A_W layer of the Al_2O_3-TiC-WC-Co composites: (a) SA2 (N_{LN} = 9, η_{TR} = 4); (b) SA4 (N_{LN} = 7, η_{TR} = 6); (c) SA5 (N_{LN} = 7, η_{TR} = 7)

Fig. 5 shows the crack propagation on the polished surface of SA2, SA4, and SA5. In all the samples, cracks propagated around the pinned particle on the polished surface, which resulted in microscale

deflection wherein the cracks met the pinned particles. In addition, bridging was observed on the polished surface of the samples. Furthermore, the propagation of cracks extended to the interior of the specimens, and partial surface bonding was observed along the cracks. The deflection, bridging, and partial surface bonding could be attributed to the residual compressive stress, which enhances the toughness of the Al_2O_3-TiC-WC-Co layered composites. The presence of Co phase in the composite leads to crack deflection because its low hardness facilitates the absorption of more fracture energy cracks, thus affecting the crack propagation path [13].

3.4. Identification and analysis of the fracture characteristic

Fig. 6 shows the relationship between the residual bending strength of SA4 and the indentation load in the *X* and *Z* directions. The variation in the bending strength of the sample with an increase in the indentation value from zero is plotted in Fig. 6. The bending strength of SA4 in the *X* and *Z* directions after loading was lesser than the original. In addition, the residual bending strength of SA4 decreased gradually with increasing indentation load, indicating that the indentation load had no significant effect on the bending strength. This tolerance corresponded to the excellent ability of the sample to resist sudden fracture, which could be attributed to the protective effect caused by the residual compressive stress [26].

Fig. 7 shows the change in the toughness curve of SA4 in the *X* and *Z* directions with an increase in the crack size using formula (3). The ψ and ξ of SA4 were 1.24 and 0.016, respectively [27]. In addition, the K_{SIN} of SA4 sharply decreased and then increased with increasing crack size, and the curve exhibited notable resistance characteristics. The gradual increase in the K_{SIN} of SA4 could be attributed to the inherent toughening effect of the sample [20], which ameliorated the resistance of the composite to crack propagation.

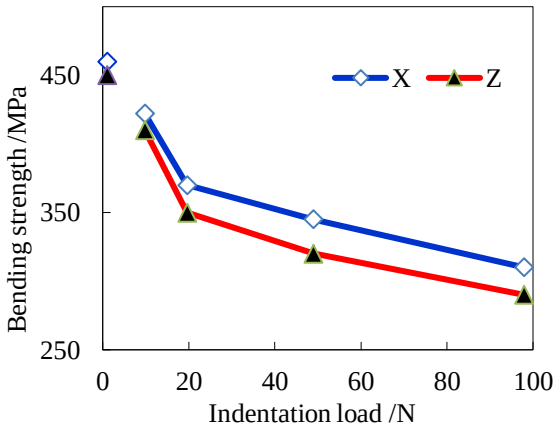

Fig. 6 Plot of the bending strength of SA4 against the indentation load

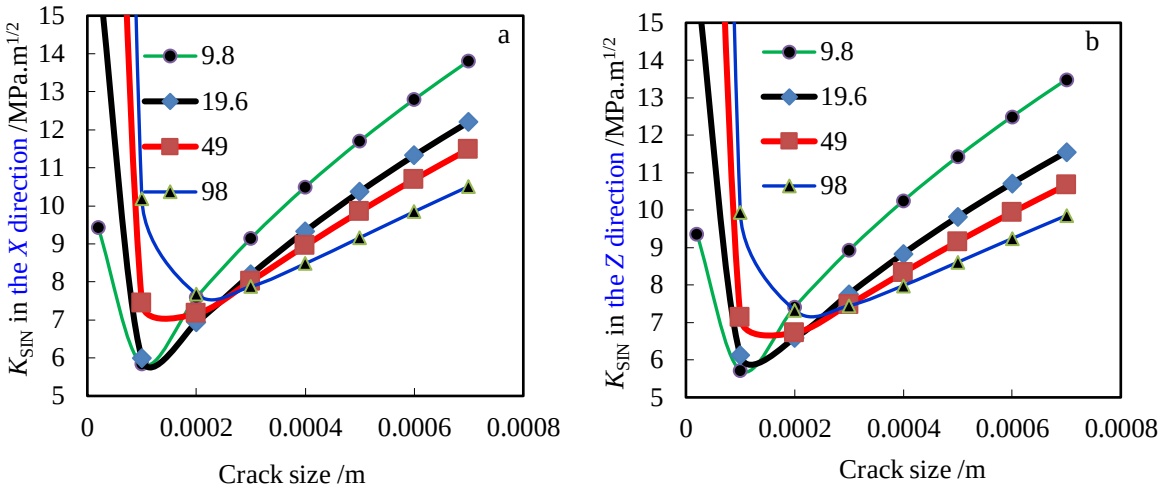

Fig. 7 Toughness curves of SA4: (a) *X* direction and (b) *Z* direction under different loads (9.8, 19.6, 49 and 98 N)

The change in the bending strength of the Al_2O_3-TiC-WC-Co layered composites with varying displacement is shown in Fig. 8. A notable elastic–plastic deformation was observed when the displacement was less than 0.05 mm, which could be attributed to the enhancement in the resistance of the layered composites to crack propagation [25, 26, 28]. In addition, the length of the terminal curve of the various layered composites was similar, and the curves of all the samples exhibited an abrupt hardening characteristic with an increase in stress after the initial slight delay (Fig. 8(b)). This characteristic could be attributed to the similar interface and residual stress in the Al_2O_3-TiC-WC-Co layered composites [26]. It was concluded that the bending strength of the Al_2O_3-TiC-WC-Co layered composite is affected by the state of interface and the distribution of the residual stresses at interface and non-interface regions.

The effect of a layered structure on the bending strength of layered composites is not clear. Some studies reported that a layered structure decreases the strength of layered composites owing to the weak interfacial adhesion between the layers of the composites [5, 11]. However, other studies found that a layered structure improves the strength of layered composites [6]. In this study, we found that the layered structure improved the strength of the Al_2O_3-TiC-WC-Co layered composites. Furthermore, the intergranular and trans-granular mixed fracture modes were found to enhance the strength of the composites. In addition, the bond strength between the interfaces of the composites was relatively high, thus leading to a fracture curve with a ductile-fracture characteristic (Fig. 8), which is consistent with the findings of a previous study [6].

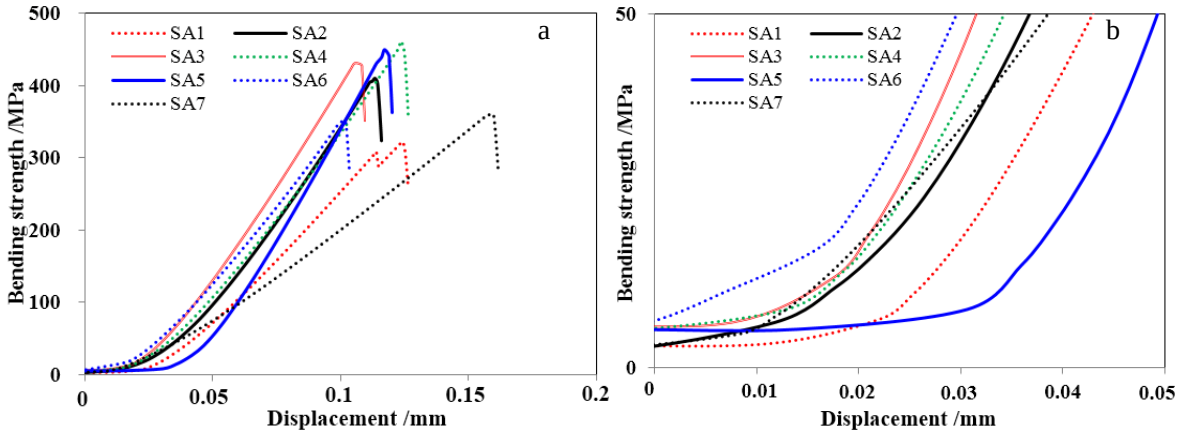

Fig. 8 Relationship between the bending strength and displacement of the Al_2O_3-TiC-WC-Co layered composites: (a) original plot and (b) enlarged plot

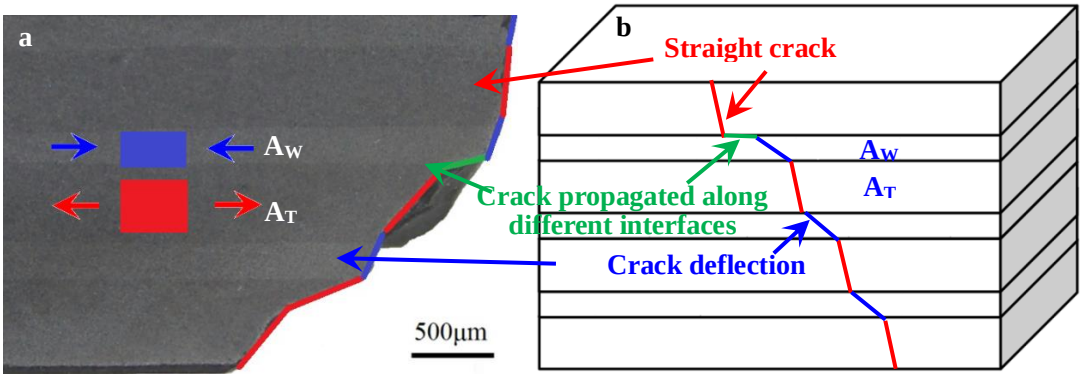

Fig. 9 Typical macrograph of the fracture surface of the Al_2O_3-TiC-WC-Co layered composite after the bending strength tests (a) and schematic model (b)

To further analyse the effect of the layered structure on the fracture mechanisms of the Al_2O_3-TiC-WC-Co composite, a typical macrograph of the fracture surface of the composite after the bending strength tests was obtained, and the schematic model of the fracture surface is shown in Fig. 9. Compared to the straight crack propagation of monolithic Al_2O_3 and Al_2O_3-TiC composites on the macroscale [20, 29], notable crack deflection occurred along with different layers in the Al_2O_3-TiC-WC-Co composite. The tensile stress in the A_T layer resulted in a small angle between the crack propagation path and the layered interface. The small angle indicated that the tensile residual stress reduced the capability of the layer to absorb fracture energy and prevented crack propagation, thus shortening the entire crack propagation path. In contrast, the compressive residual stresses in the A_W layer resulted in a larger angle, which was considered as the effective toughening mechanism in the layered composites. This is because the residual stress increased the crack propagation length, thus enhancing the ability of the layer to absorb fracture energy during the fracture process. In addition, the crack propagated along with different interfaces,

indicating that the bond strength between the interfaces was weaker than the strength inside the layer (Fig. 9). This implies that the weak interface bonding in the Al_2O_3-TiC-WC-Co layered composite facilitated the absorption of fracture energy by the composite.

The effect of the crack size on the critical stress at the crack tip, σ_c, was calculated using the following formula [30]:

$$\sigma_C = [E \cdot Q_p / (\prod \cdot c)]^{1/2}, \quad (7)$$

where Q_p is a constant related to the fracture energy. Formula (7) indicates that σ_c decreases with an increase in c. The intergranular fracture of the A_W layer resulted in a relatively longer crack propagation path, thus significantly reducing the possibility of sudden fracture in the Al_2O_3-TiC-WC-Co layered composite with an increase in the length of the crack propagation path.

Several factors contributed to the amelioration of the crack propagation ability of the Al_2O_3-TiC-WC-Co layered composites, such as (1) mismatch in the CTEs of the matrix and additives, particularly, the residual compressive stress, (2) multiple interfaces caused by the layered structure of the composite, and the interface bonding state, which resulted in the deviation of the crack propagation path from the original path when it crossed the interface, and (3) combination of the trans-granular and intergranular fracture modes in the composites. Thus, the gradual increase in the K_{SIN} of the composites with an increase in the crack size could be attributed to the aforementioned factors at the micro and macro levels.

The lateral crack propagation and the intersection of the surface according to the Marshall indentation theory are shown in Fig. 10. The height, h, and lateral crack length, C_L, of the plastic zone were calculated using the following formulas [31]:

$$h \propto \frac{\sin\theta^{1/3}\mu}{\alpha^{1/6}} \frac{E^{1/2}}{H^{5/6}} U^{1/3} \alpha^{1/6}, \quad (8)$$

$$C_L = (3^{5/6} \frac{\alpha^{5/12}\zeta_L}{A^{1/2}} \frac{E^{3/4}}{K_{IC}{}^{1/2} H^{7/12}} U^{5/6})^{1/2} [1 - (\frac{1}{3^{1/6}} \frac{\zeta_o{}^{1/4}}{\alpha^{1/12} A^{1/2}} \frac{E^{1/4} K_{IC}}{H^{13/12} U^{1/6}})]^{1/2}, \quad (9)$$

where θ is the angle of the indentation tip, U is the energy absorbed by the indented material, and ζ_L, ζ_o, α, μ, and A are constants. The relationship between the mechanical properties and volume of the plastic zone, V_P, can be expressed using the following equation [31]:

$$V_p \propto \frac{\rho_t E^{5/4}}{H^{5/2} K_{IC}} (3A^{1/2} H^{13/12} \alpha^{1/12} U^{1/6} - 3^{5/6} \zeta_L{}^{1/4} K_{IC} E^{1/4}), \quad (10)$$

where ρ_t is the density of the Al_2O_3-TiC-WC-Co layered composites.

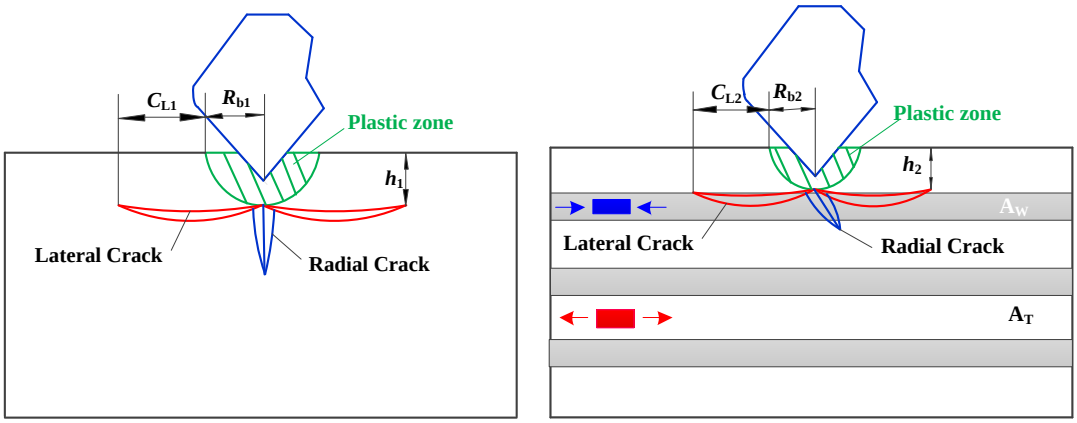

Fig. 10 Schematic illustration of the formation of lateral crack and radial crack in (a) monolithic Al_2O_3 composite and (b) Al_2O_3-TiC-WC-Co layered composite (C_L: lateral crack length, R_b: plastic zone)

According to formula (10), V_p decreased with an increase in K_{IC}, which was accompanied by a decrease in h and C_L. This indicates that the layered structure had a positive significant effect on the fracture toughness of the composites and a deleterious effect on its hardness. Formula (10) indicates that in comparison to the monolithic Al_2O_3 composite, the Al_2O_3-TiC-WC-Co layered composite absorbed more energy, which resulted in a decrease in the volume of its plastic zone (Fig. 10). Meanwhile, a lower V_p corresponded to a high fracture resistance of the Al_2O_3-TiC-WC-Co layered composite. It was confirmed that the radial crack in the Al_2O_3-TiC-WC-Co layered composite was influenced by the compressive stress state (Fig. 10(b)). This provided a new theoretical perspective for describing the mechanism of the effect of the layered structure on the fracture toughness of composites for the prevention of fracture.

4. Conclusion

In this study, the structural design, microstructure, and mechanical performance of Al_2O_3-TiC-WC-Co layered composites, particularly, their fracture behaviour in the X and Y directions, were investigated. The following three conclusions were drawn.

(1) SA4 (N_{LN} = 7, η_{TR} = 6) achieved bending strengths of 460 and 450 MPa in the X and Z directions, respectively, which were the highest among the analysed samples. In addition, the fracture toughness and hardness of SA4 in the A_T layers and A_W layers were 8.5 and 8.4 MPa·m$^{1/2}$ and 21.5 and 22.2 GPa, respectively.

(2) The enhancement in the bending strength of the Al_2O_3-TiC-WC-Co layered composite could be attributed to the combination of the intergranular (A_T layer) and trans-granular (A_W layer) fracture modes, layered structure, interface bonding state, and distribution of residual stress. In addition, the gradual

increase in the K_{SIN} of the Al_2O_3-TiC-WC-Co layered composites with an increase in the crack size could be attributed to a combination of microscale and macroscale factors. Furthermore, the tensile residual stress in the A_T layers resulted in a straight crack propagation path, whereas the compressive residual stresses in the A_W layers resulted in a notable crack deflection and partial surface bonding.

(3) A new perspective was proposed to describe the mechanism of the effect of the layered structure on the fracture toughness of the layered composites. In addition, a schematic illustration of the formation of lateral and radial cracks in the Al_2O_3-TiC-WC-Co layered composites was proposed. The results revealed that the radial crack in the composite was influenced by the presence of compressive stress.

Acknowledgements

The authors are grateful to the financial support from National Natural Science Foundation of China (Grant No. 51505208 and 51475222), Key Technology Research and Development Program of Shandong province (Grant No. 2019GGX104085) and Scientific Research Projects in University of Shandong province (Grant No. J18KA031).

Reference

[1] Mengyong Sun, Yuhang Bai, Mingxing Li, et al. Structural design of laminated B_4C/TiC composite fabricated by reactive melt infiltration, Journal of Alloys and Compounds, 765 (2018) 913-920.

[2] Yuhang Bai, Mengyong Sun, Mingxing Li, et al. Comparative evaluation of two deferent methods for thermal shock resistance of laminated ZrB_2-SiCw/BN ceramics, Ceramics International, 44 (2018) 19686-19694.

[3] Xuefeng Yang, Ziran Wang, Peilong Song, et al. Laminated structure optimization and drawing performance of Al_2O_3-TiC/Al_2O_3-TiC-CaF_2 self-lubricating laminated ceramic conical die, Ceramics International, 41 (2015) 12480-12489.

[4] Goffredode Portu, Paola Pinasco, Cesare Melandri, et al. Solid particle erosion behavior of laminated ceramic structures, Wear, 2020, 442-443, 203147.

[5] Yuanyuan Li, Qinggang Li, Zhi Wang, et al. Fabrication of laminated ZrB_2-SiC ceramics via tape casting and vacuum hot-pressing sintering and their mechanical properties, Ceramics International, 41 (2015) 11555-11561.

[6] Shuo Chen, Zhongminzhao, Xuegang Huang, et al. Interfacial microstructure and mechanical properties of laminated composites of TiB_2-based ceramic and 42CrMo alloy steel. Materials Science and Engineering A, 674 (2016) 335-342.

[7] Chuncheng Wei, Xinchao Liu , Jinye Niu, et al. High temperature mechanical properties of laminated ZrB_2-SiC based ceramics, Ceramics International, 42 (2016) 18148-18153.

[8] Youde Tan, Hongnian Cai, Xingwang Cheng, et al. Microstructural and mechanical properties of in-situ micro-laminated TiC/Ti composite synthesised, Materials Letters, 228 (2018) 1-4.

[9] Yupeng Xie, Laifei Cheng, Hui Mei, et al. Effect of SiC particles on mechanical properties of laminated (SiCw+SiCp)/SiC ceramic composites, International Journal of Applied Ceramic Technology, 12 (3) (2015) 535-541.

[10] Xinchao Liu, Chuncheng Wei, Liu Feng, et al. R-curve behavior of laminated ZrB_2-SiC/Graphite ceramics in two different directions, Ceramics International, 43 (2017) 6612-6617.

[11] Kai Cui, Yongkui Li. Fabrication, mechanical properties and thermal shock resistance of laminated TiB_2-based ceramic, International Journal of Refractory Metals & Hard Materials, 54 (2016) 148-153.

[12] Deng Jianxin, Duan Zhenxing, Yun Dongling, Zhang Hui, Ai Xing, Zhao Jun. Fabrication and performance of Al_2O_3/(W,Ti)C +Al_2O_3/TiC multilayered ceramic cutting tools, Materials Science and Engineering A, 527 (2010) 1039–1047.

[13] Xianhua Tian, Kuicheng Yan, Hao Liu, Jun Zhao, Jinyong Yang. Effect of Co on thermal and mechanical properties of Si_3N_4 based ceramic tool material, Ceramics International, 45 (2019) 19435–19441.

[14] Changxia Liu, Junlong Sun, Gang Li, Bin Li, Feng Gong. Fabrication, mechanical properties and fracture behaviors of the laminated Al_2O_3-ZrB_2-MgO / Al_2O_3-TiN-MgO ceramic composite, Ceramics International, 46 (2020) 857-865.

[15] A. G. Evans, M. E. Gulden, Rosenblatt. Impact Damage in Brittle Materials in the Elastic-Plastic Response Régime, Proceedings of the Royal Society of London. Series A, Mathematical and Physical Sciences, 361 (1978) 343-365.

[16] R.F. Cook, B.R. Lawn, A modified indentation toughness technique, Journal of the American Ceramic Society, 66 (11) (1983) 200-201.

[17] Linda M. Braun, Stephen J. Bemison, and Brian R. Lawn. Objective evaluation of Short-Crack toughness curves using indentation flaws: case study on alumina-based ceramics, Journal of the American Ceramic Society, 75 (11) (1992) 3049-3057.

[18] S. M. Smith, R. O. Scattergood, Crack-shape effects for indentation fracture toughness measurements, Journal of the American Ceramic Society, 75 (2) (1992) 305-315.

[19] Y.-W. Mai and B. R. Lawn, Crack stability and toughness characteristics in brittle materials, Annual Review of Materials Research, 16 (1986) 415-39.

[20] R. F. Cook, C. J. Fairbanks, B. R. Lawn, and Y -W. Mai, Crack resistance by interfacial bridging: its role in determining strength characteristics, Journal of Materials Research, 2(3) (1987) 345-356.

[21] Jianghong Gong, Zhe Zhao, Hezhuo Miao, et al. R-curve behavior of TiC particle reinforced Al_2O_3 composites, Scripta Materialia, 43 (1) (2000) 27-31.

[22] Oel HJ, Fréchette VD. Stress distribution in multiphase systems: I, composites with planar interfaces. Journal of the American Ceramic Society, 50 (1967) 542-549.

[23] Lubo Náhlík, Katerina tegnerová, Bohuslav Máa, et al. A failure scenario of ceramic laminates with strong interfaces, Engineering Fracture Mechanics, 167 (2016) 56-67.

[24] J. Hausmann, P. Naghipour, K. Schulze. Analytical and numerical residual stress models for fiber metal laminates -comparison and application, Procedia Materials Science, 2 (2013) 68-73.

[25] Jianghong Gong, Zhe Zhao, Zhenduo Guan. On the local crack resistance of Al_2O_3-TiC composites evaluated by direct indentation method, Journal of the European Ceramic Society, 21 (7) (2001) 941-946.

[26] Liangjun Li, Laifei Cheng, Shangwu Fan, et al. Effect of large thicknesses on the characteristics of laminated ZrO-Zr_2CN-Si_3N_4 ceramics by reactive hot pressing, Journal of Alloys and Compounds, 656 (2016) 654-662.

[27] Peng Zhou, Ping Hu, Xinghong Zhangb, et al. R-curve behavior of laminated ZrB_2-SiC ceramic with strong interfaces, Interntional Journal of Refractory Metals and Hard Materials, 52 (2015) 12-16.

[28] A. Evans, Z. Suo, R. Wang, I. Aksay, M. He, J. Hutchinson, Model for the robust mechanical behavior of nacre, Journal of Materials Research, 16 (9) (2001) 2475-2484.

[29] Zengbin Yin, Chuanzhen Huang, Bin Zou, et al. Dynamic fatigue behavior of Al_2O_3/TiC micro-nano-composite ceramic tool materials at ambient and high temperatures, Materials Science & Engineering A, 593 (2014) 64-69.

[30] Maleki, Mohammad Sheikh-Al-Eslamian, Seyedeh Mahsa Hasani, et al. Comparative study on the microstructure and mechanical behavior of monolithic ceramic and laminated composite of high strength 3Y-TZP and high fracture toughness 12Ce-TZP, Journal of Alloys and Compounds, 776 (2019) 166-171.

[31] Sun Junlong, Liu Changxia, Lin Hongqi, et al. Effect of mechanical properties and impact angles on erosion behavior of B_4C/TiB_2 matrix ceramic nozzle materials. Ceramics International, 42(7) (2016) 8826-8832.